

Quantum corrections to a spin-orbit-coupled Bose-Einstein condensate

Long Liang^{1,2} and Päivi Törmä¹

¹*Department of Applied Physics, Aalto University School of Science, FI-00076 Aalto, Finland*

²*Computational Physics Laboratory, Physics Unit, Faculty of Engineering and Natural Sciences, Tampere University, P.O. Box 692, FI-33014 Tampere, Finland*



(Received 19 March 2019; revised manuscript received 24 May 2019; published 22 August 2019)

We study systematically the quantum corrections to a weakly interacting Bose-Einstein condensate with spin-orbit coupling. We show that quantum fluctuations, enhanced by the spin-orbit coupling, modify quantitatively the mean-field properties such as the superfluid density, spin polarizability, and sound velocity. We find that the phase boundary between the plane wave and zero momentum phases is shifted to a smaller transverse field. We also calculate the Beliaev and Landau damping rates and find that the Landau process dominates the quasiparticle decay even at low temperature.

DOI: [10.1103/PhysRevA.100.023619](https://doi.org/10.1103/PhysRevA.100.023619)

I. INTRODUCTION

The spin-orbit coupling, arising due to the interaction of a particle's spin with its motion in an electric field plays a crucial role in various branches of physics, including topological insulators [1,2], topological semimetals [3,4], and Majorana fermions [5]. In bosonic systems, the interplay of the interparticle interaction and spin-orbit coupling gives rise to exotic Bose-Einstein condensates, which have been investigated in a rich variety of systems, including magnons [6–8], excitons [9–12], exciton-polaritons [13–18], and ultracold atoms [19–22].

For a weakly interacting Bose-Einstein condensate, the mean-field theory provides a reliable description of various physical properties [23]. To reveal beyond mean-field effects, one method is to reach the strongly interacting regime, which can be achieved in exciton-polaritons because of the strong coupling between the exciton and photon [13,24–27], and for ultracold atoms strong interactions are accessible by means of Feshbach resonances [28–30]. However, strong interactions reduce the lifetime of Bose-Einstein condensates significantly. Another method is to fine tune the interaction parameters such that the mean-field interactions almost cancel out [31–35], making the quantum fluctuations unmasked. The spin-orbit coupling provides an alternative way to enhance interaction effects due to the increased density of states [36]. However, only a handful of theoretical studies have addressed the beyond mean-field effects [37–41], and a thorough analysis of the quantum fluctuations in spin-orbit coupled bosonic systems is still lacking.

In this paper, we systematically investigate the quantum corrections to a spin-orbit coupled Bose-Einstein condensate. We study a model system that is simple and general, potentially realizable in various platforms, and already implemented with ultracold atom experiments [19–21]. The model shows three novel condensation phases [19,42], namely the stripe, plane wave, and zero momentum phases. To demonstrate the interplay between interaction and spin-orbit coupling, we focus on the zero momentum phase, which is the

simplest case capturing the essential physics of spin-orbit coupling and interactions.

We calculate quantum corrections to a number of physical properties, including the superfluid density, spin polarizability, and sound velocity. The superfluid density at the mean-field phase transition point between the plane wave and zero momentum phases becomes nonzero due to quantum fluctuations, and as a result, the phase transition point is shifted towards a smaller transverse field. The spin polarizability diverges at the corrected phase transition point but remains finite at the mean-field phase boundary, which seems to be consistent with a recent experiment [20]. The sound velocity also acquires quantitative corrections, which may be detected in current ultracold atom experiments and provides a way to explore the beyond mean-field effects. Finally, we obtain an analytical result for the Landau decay rate of phonons at low temperature. Unlike the Beliaev decay predicted in Ref. [41], the Landau damping is not suppressed in the direction of spin-orbit coupling, making it the dominant mechanism for the quasiparticle decay.

II. MODEL SYSTEM

We consider a generic model of a spin-1/2 Bose gas with spin-orbit coupling, described by the single-particle Hamiltonian (we set $\hbar = m = 1$)

$$h_0 = \frac{(p_x - k_0 \sigma_z)^2 + p_y^2 + p_z^2}{2} + \frac{\Omega}{2} \sigma_x, \quad (1)$$

where σ_i with $i = x, y, z$ are the 2×2 Pauli matrices. The one-dimensional spin-orbit coupling, characterized by k_0 , appears in many realistic systems, including ultracold gases [19–21,43,44] and semiconducting nanowires [45–47]. The model applies to several systems but to compare with experiments, we consider the cold atom setup where k_0 is given by the momentum transfer from the two Raman laser beams and Ω is the Rabi frequency of the Raman beams. The interaction

between the particles can be written as

$$H_{\text{int}} = \frac{1}{2} \sum_{\sigma\sigma'} \int d^3\mathbf{r} g_{\sigma\sigma'} n_{\sigma}(\mathbf{r}) n_{\sigma'}(\mathbf{r}), \quad (2)$$

where n_{σ} is the density of particles with spin $\sigma = \uparrow, \downarrow$, and $g_{\sigma\sigma'} = 4\pi a_{\sigma\sigma'}$ are the interaction strengths in different spin channels, with $a_{\sigma\sigma'}$ being the corresponding s -wave scattering lengths in case of ultracold quantum gases. In the following we assume $g_{\uparrow\uparrow} = g_{\downarrow\downarrow} \equiv g$ and $g_{\uparrow\downarrow} \equiv g'$, and correspondingly, $a_{\uparrow\uparrow} = a_{\downarrow\downarrow} \equiv a$ and $a_{\uparrow\downarrow} \equiv a'$. It is convenient to define interaction parameters $G_1 = g_+\rho$ and $G_2 = g_-\rho$ with $g_{\pm} = (g \pm g')/2$ and $\rho = N/V$ being the total particle density. In recent experiments [19–21], ^{87}Rb atoms are employed and the interaction is almost $SU(2)$ invariant, with $G_2/G_1 \approx 10^{-3}$. The typical interaction parameter is $G_1 \approx 0.24k_0^2$ with the peak density $\rho \approx 0.57k_0^3$ [20]. The dimensionless parameter $\sqrt{a^3\rho} \approx 0.004$ is small, ensuring that the condensate is in the weakly interacting regime and the perturbation calculations are controlled.

The mean-field phase diagram of this model has been extensively investigated, for a review see Ref. [36]. For small Rabi frequency, the condensate wave function is a superposition of two plane waves with different momenta, characterizing the stripe phase with density modulations in the ground state. In this phase, both the translational and $U(1)$ symmetries are broken, and therefore there are two branches of gapless excitations. Increasing the Rabi frequency Ω , the system enters the plane wave phase, in which the bosons condense in a single plane wave state. There is only one branch of gapless excitations in this phase and the energy dispersion contains a roton minimum at finite momentum. Further increasing the Rabi frequency such that $\Omega > \Omega_{c,\text{mf}} \equiv 2k_0^2 - 2G_2$, the system enters the zero momentum phase, where the roton minimum disappears and the phonon excitation spectrum resembles that of a Bose-Einstein condensate without spin-orbit coupling. To reveal the essential effect of interactions, we focus on the simplest zero momentum phase to reduce the effect of nontrivial mean-field energy dispersions in the plane wave and stripe phases.

The ground-state wave function for the zero momentum phase is described by a spinor $\psi = \sqrt{\rho/2}[1, -1]^T$. To characterize excitations on top of the condensate, we introduce phase and number fluctuations, and write the spinor field as

$$\psi = \frac{e^{i\phi}}{\sqrt{2}} \begin{bmatrix} \sqrt{\rho + \zeta_1} e^{i\varphi} \\ -\sqrt{\rho + \zeta_2} e^{-i\varphi} \end{bmatrix}, \quad (3)$$

where ϕ is the total and φ is the relative phase fluctuations of the condensate, and ζ_1 and ζ_2 are the density fluctuations for spin-up and spin-down particles, respectively.

We use the imaginary time path integral formalism. The Lagrangian density is obtained through the Hamiltonian as

$$\mathcal{L} = \psi^\dagger (\partial_\tau + h_0 - \mu) \psi + \frac{g_+}{2} (\psi^\dagger \psi)^2 + \frac{g_-}{2} (\psi^\dagger \sigma_z \psi)^2, \quad (4)$$

with μ being the chemical potential. It is convenient to introduce the density and spin fluctuations, $\zeta_+ = (\zeta_1 + \zeta_2)/2$ and $\zeta_- = (\zeta_1 - \zeta_2)/2$, which are conjugate to ϕ and φ , respectively. We then expand \mathcal{L} in terms of the new variables, and up



FIG. 1. Feynman diagrams for diagonal elements of the mean-field Green's function.

to the second order, we get the mean-field Lagrangian density

$$\mathcal{L}_{\text{mf}} = \left(G_1 + \frac{k_0^2 - \Omega}{2} - \mu \right) \zeta_+ - \mu \rho + \frac{g_+\rho^2}{2} + \frac{1}{2} [\phi, \zeta_+, \varphi, \zeta_-] \mathcal{G}_0^{-1} [\phi, \zeta_+, \varphi, \zeta_-]^T, \quad (5)$$

where the mean-field Green's function in the momentum and frequency representation is

$$\mathcal{G}_0^{-1}(i\omega_n, \mathbf{q}) = \begin{bmatrix} \mathcal{A}(\mathbf{q}) & -\omega_n & 0 & -ik_0q_x \\ \omega_n & \mathcal{B}(\mathbf{q}) & ik_0q_x & 0 \\ 0 & -ik_0q_x & \mathcal{C}(\mathbf{q}) & -\omega_n \\ ik_0q_x & 0 & \omega_n & \mathcal{D}(\mathbf{q}) \end{bmatrix}, \quad (6)$$

where $\omega_n = 2\pi nT$ is the Matsubara frequency (we set $k_B = 1$), $\mathcal{A}(\mathbf{q}) = \rho\mathbf{q}^2$, $\mathcal{B}(\mathbf{q}) = \mathbf{q}^2/(4\rho) + g_+$, $\mathcal{C}(\mathbf{q}) = \rho\mathbf{q}^2 + 2\Omega\rho$, and $\mathcal{D}(\mathbf{q}) = \mathbf{q}^2/(4\rho) + g_- + \Omega/(2\rho)$. The chemical potential is determined by requiring $\langle \zeta_+ \rangle = 0$, and at the mean-field level we find $\mu = G_1 + (k_0^2 - \Omega)/2$, so the first-order term of ζ_+ vanishes and the mean-field Lagrangian density is quadratic. The diagonal elements of \mathcal{G}_0 are represented by Feynman diagrams shown in Fig. 1.

III. MEAN-FIELD RESULTS

Before studying the beyond mean-field corrections, we first present the mean-field predictions of the physical properties we are interested in. These results are readily obtained from the mean-field Green's function.

The mean-field excitation energy is determined by $\det \mathcal{G}_0^{-1} = 0$. In the low momentum limit, we find the gapless phonon dispersion to be

$$\varepsilon_{\text{ph}} = c_0 \sqrt{q^2 - \frac{2k_0^2 q_x^2}{\Omega + 2G_2}} = c_0 q \sqrt{1 - \frac{2k_0^2 \cos^2 \theta}{\Omega + 2G_2}} \equiv c_\theta q, \quad (7)$$

where $c_0 = \sqrt{G_1}$ and c_θ is the sound velocity, which depends on the angle θ between the directions of the momentum \mathbf{q} and the x axis. The mean-field sound velocities c_y and c_z are the same as the usual Bogoliubov sound velocity c_0 . An intriguing feature is that the mean-field sound velocity in the x direction, c_x , vanishes at the phase transition point between the plane wave and zero momentum phases. Besides the gapless phononic mode, there also exists a gapped mode, which is dominated by spin excitation, with the mean-field gap given by $\Delta_0 = \sqrt{\Omega(\Omega + 2G_2)}$.

The density and spin response functions are given by the Green's functions $\mathcal{G}_{\zeta_+\zeta_+}$ and $\mathcal{G}_{\zeta_-\zeta_-}$, respectively. From the spin response function, the spin polarizability [48,49] can be obtained, and at the mean-field level, we get

$$\chi_M = \mathcal{G}_{0,\zeta_-\zeta_-}(q_x \rightarrow 0)/\rho = \frac{2}{\Omega - \Omega_{c,\text{mf}}}, \quad (8)$$

which diverges at the mean-field phase transition point.

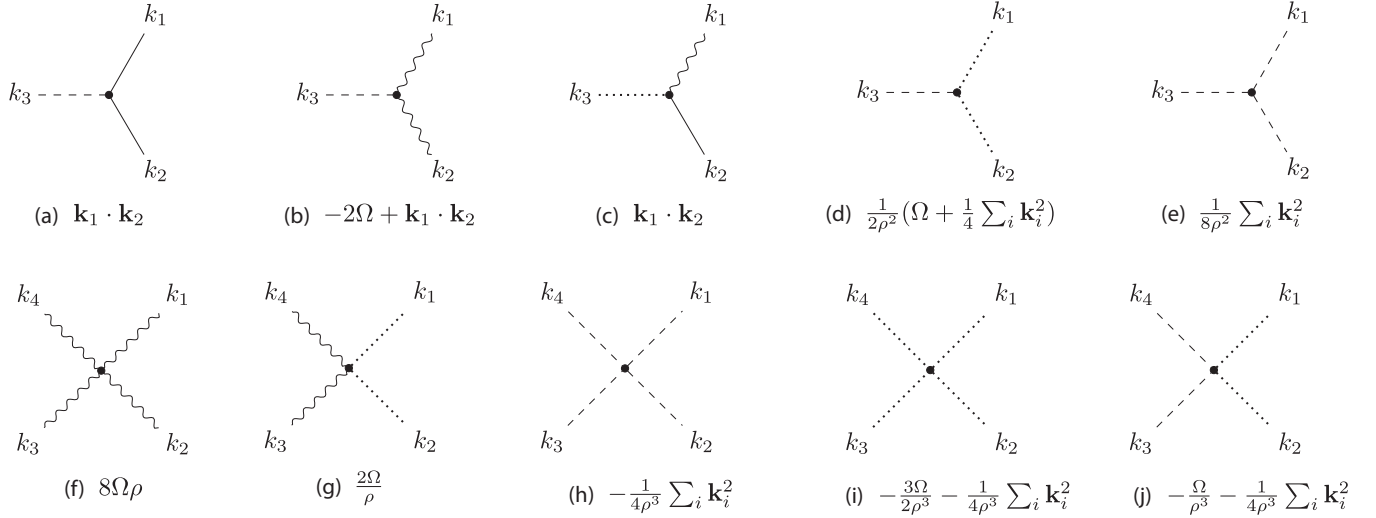


FIG. 2. Feynman diagrams for interaction vertices.

An important quantity characterizing superfluidity is the superfluid density, which governs the total phase fluctuations. To get the superfluid density, we integrate out the φ , ζ_- , and ζ_+ fields and obtain an effective theory of ϕ (see Appendix A). In the low-energy and long-wavelength limit, we find

$$\mathcal{L}_{\text{eff}} = (K\omega_n^2 + \rho_i q_i^2) |\phi|^2, \quad (9)$$

where K is the zero momentum static density response function with its mean-field value being $1/g_+$, and $\rho_y = \rho_z = \rho$, $\rho_x = \rho[1 - 2k_0^2/(\Omega + 2G_2)]$ are the mean-field superfluid densities. From the effective Lagrangian, we see that the sound velocity is related to the superfluid density through $c_i = \sqrt{K^{-1}\rho_i}$.

Note that the superfluid density in the x direction vanishes when $\Omega = 2k_0^2 - 2G_2$. Formally, for smaller Ω , the superfluid density becomes negative, which means that a state with nonzero phase gradient, i.e., the plane wave phase, is energetically

more favorable. In other words, a vanishing superfluid density indicates a second-order phase transition from the zero momentum phase to the plane wave phase.

In Ref. [50], the superfluid density ρ_x is calculated from the current-current correlation function, which can be written in terms of the transverse spin polarization $\langle \sigma_x \rangle$ and the excitation gap Δ as $\rho_x = \rho(1 + 2k_0^2\Omega\langle \sigma_x \rangle/\Delta^2)$. Substituting the mean-field values $\Delta = \Delta_0$ and $\langle \sigma_x \rangle = -1$, we obtain from this the same result as given by the effective theory method above. Note that if the gap becomes larger or σ_x is not fully polarized, the superfluid density ρ_x will increase.

IV. BEYOND MEAN-FIELD CORRECTIONS

To study the lowest order (one-loop) beyond mean-field corrections, we expand the Lagrangian density up to the fourth order of the fields,

$$\begin{aligned} \mathcal{L}_{\text{fluct}} = & \frac{\zeta_+}{2} [(\nabla\phi)^2 + (\nabla\varphi)^2] + \zeta_- \nabla\phi \nabla\varphi - \frac{\Omega\rho}{3} \varphi^4 + \Omega\zeta_+ \varphi^2 - \frac{\Omega}{2\rho} \zeta_-^2 \varphi^2 - \frac{\Omega}{2} \left(\frac{\zeta_+ \zeta_-^2}{2\rho^2} - \frac{\zeta_-^2 \zeta_+^2}{2\rho^3} - \frac{\zeta_-^4}{8\rho^3} \right), \\ & - \frac{\zeta_+ [(\nabla\zeta_+)^2 + (\nabla\zeta_-)^2]}{8\rho^2} - \frac{\zeta_- \nabla\zeta_+ \nabla\zeta_-}{4\rho^2} + \frac{(\zeta_+^2 + \zeta_-^2) [(\nabla\zeta_+)^2 + (\nabla\zeta_-)^2] + \nabla\zeta_+^2 \nabla\zeta_-^2}{8\rho^3}. \end{aligned} \quad (10)$$

The Feynman diagrams corresponding to the vertices are given in Fig. 2. Without the spin-orbit coupling, the one-loop corrections can be calculated analytically, and the results are given in Appendix B. In the main text we focus on the more interesting situation with nonzero spin-orbit coupling and calculate the one-loop corrections numerically. Since the parameter G_2 is small, we take it to be zero unless otherwise mentioned.

A. Quantum depletion

Due to the quantum fluctuations, the condensate is depleted by a fraction of the total density. Up to the lowest order, the

quantum depletion is given by (see Appendix B)

$$\delta\rho = \rho(\langle \phi^2 \rangle + \langle \varphi^2 \rangle) + \frac{\langle \zeta_+^2 \rangle + \langle \zeta_-^2 \rangle}{4\rho}. \quad (11)$$

Figure 3 shows the quantum depletion as a function of the interaction strength and spin-orbit coupling for different transverse fields. The quantum depletion increases with the interaction strength. We find that it also increases with the spin-orbit coupling strength, which is consistent with previous results [37,38]. As Fig. 3 shows, the quantum depletion increases with decreasing Ω , which means that the quantum fluctuations are enhanced as the system approaches the phase transition point.

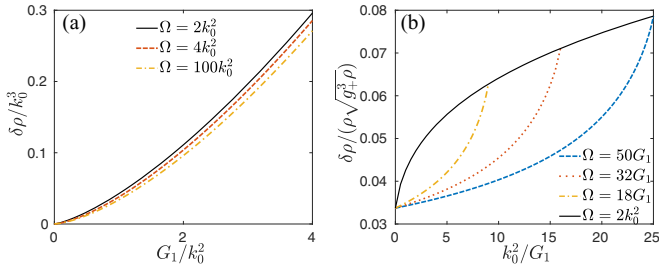


FIG. 3. The quantum depletion as a function of (a) the interaction and (b) spin-orbit coupling for different Raman fields Ω . The solid lines correspond to the mean-field phase transition between the zero momentum and plane wave phases.

B. Lee-Huang-Yang correction and chemical potential shift

We study the correction to the mean-field energy density, which is known as the Lee-Huang-Yang (LHY) correction [51] \mathcal{E}_{LHY} , and can be viewed as the zero point energy of the excitations [52]. With increasing k_0 , the phonon mode softens, and therefore the zero point energy decreases. Figure 4(a) shows this behavior clearly. Remarkably, we find that \mathcal{E}_{LHY} becomes negative for large enough spin-orbit coupling. This leads to a nonmonotonic dependence of \mathcal{E}_{LHY} on G_1 : If we fix k_0 and increase G_1 from zero, then for small G_1 (large k_0^2/G_1), the LHY correction decreases from zero to negative; increasing G_1 further, the LHY correction will increase since it becomes positive for small k_0^2/G_1 . The nonmonotonic behavior of \mathcal{E}_{LHY} is most clearly seen at the phase transition point, see Fig. 4(b).

We then calculate the correction to the chemical potential, which is given by the tadpole diagrams shown in Fig. 5. The numerical results of $\delta\mu$ are shown in Figs. 4(c) and 4(d). As the LHY correction, the chemical potential shift decreases with increasing of k_0 and depends nonmonotonically on G_1 .

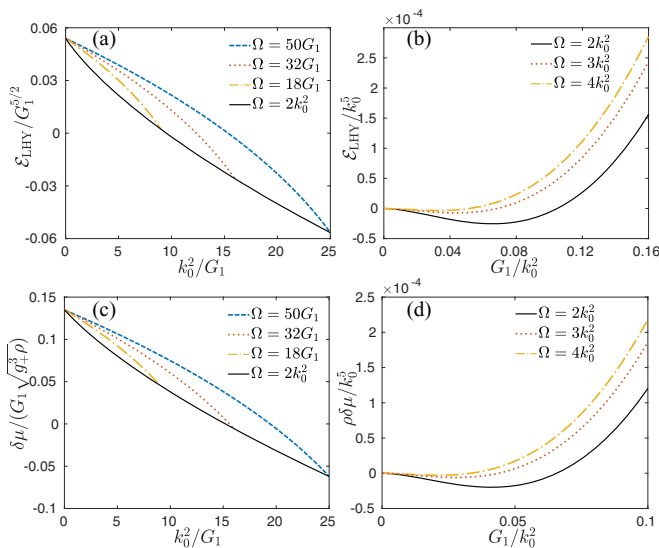


FIG. 4. (a), (b) The LHY correction and (c), (d) the chemical potential shift as a function of the spin-orbit coupling and interaction for different Raman fields Ω . The value $\Omega = 2k_0^2$ corresponds to the mean-field phase transition.

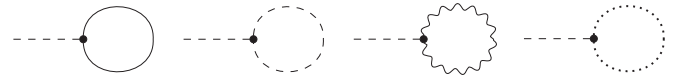


FIG. 5. Feynman diagrams that determine the chemical potential shift $\delta\mu$. These tadpole diagrams are canceled by the chemical potential shift and therefore do not contribute to the one-loop self-energy. For notation see Fig. 1.

This is expected, because the chemical potential shift can also be obtained as the first-order derivative of the LHY energy with respect to the density.

C. Superfluid density, phase boundary shift, and spin polarizability

To get the correction to the superfluid density, we first calculate the one-loop self-energy and then integrate out the massive fields φ , ζ_- , and ζ_+ to get the effective Lagrangian of the total phase fluctuations. The superfluid density in the x direction is found to be

$$\rho_x = \rho \left[1 - \frac{2k_0^2}{\Omega + 2G_2 - 2\rho \Sigma_{\zeta-\zeta_-}(0)} \right], \quad (12)$$

where $\Sigma_{\zeta-\zeta_-}(0)$ is the self-energy at zero frequency and momentum. There is no correction to ρ_y and ρ_z at zero temperature, consistent with the general result of superfluid density in Galilean invariant superfluids [53].

Our numerical calculations show that $\Sigma_{\zeta-\zeta_-}(0)$ is nonzero at the mean-field transition point. Consequently, the superfluid density also becomes nonzero at $\Omega = \Omega_{c,\text{mf}}$, see Fig. 6(a). Physically, this can be explained by the decrease of the

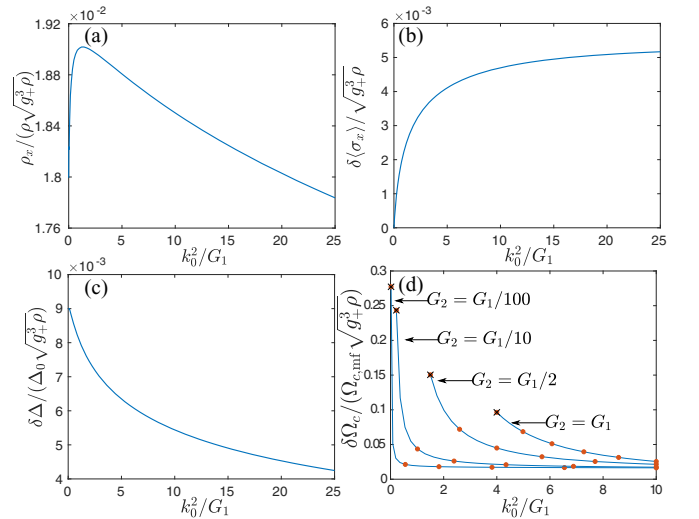


FIG. 6. (a) The superfluid density, (b) the deviation of the transverse spin polarization, (c) and the spin excitation gap at the phase transition point. (d) The phase boundary shift as a function of k_0^2/G_2 for different G_2/G_1 . Here $\delta\Omega_c = \Omega_{c,\text{mf}} - \Omega_c$, with Ω_c being the corrected phase boundary. The solid lines show the results determined by the one-loop superfluid density, and the dots present the results by minimizing the ground-state energy $\mathcal{E}_{\text{mf}} + \mathcal{E}_{\text{LHY}}$. The crosses denote the mean-field critical $k_{0,c}$ below which the plane wave phase is preempted by the stripe phase [42].

transverse polarization $\langle\sigma_x\rangle$ and the increase of the spin gap Δ . Because of the spin-orbit coupling, the spin of excited particles is not perfectly along the x direction, and therefore the magnitude of the transverse spin polarization is reduced. Up to the lowest order, the deviation of spin polarization is (see Appendix B)

$$\delta\langle\sigma_x\rangle = 2\langle\varphi^2\rangle + \frac{\langle\xi_-^2\rangle}{2\rho^2}. \quad (13)$$

We plot the numerical result of $\delta\langle\sigma_x\rangle$ in Fig. 6(b). Another quantity that determines ρ_x is the excitation gap. We obtain from the one-loop self-energy the correction to the mean-field gap and find it is positive, see Fig. 6(c). Combining the behavior of $\delta\langle\sigma_x\rangle$ and Δ , the nonmonotonic dependence of ρ_x on k_0^2 can be explained: The superfluid density increases with increasing $\delta\langle\sigma_x\rangle$ and Δ , and with increasing k_0 , $\delta\langle\sigma_x\rangle$ increases but Δ decreases. As a result, the superfluid density first increases and then decreases with increasing the spin-orbit coupling strength.

As we have explained before (see also Appendix C), the phase transition between the zero momentum and plane wave phases is characterized by the vanishing superfluid density, so Eq. (12) means that the phase transition point is shifted by quantum fluctuations. The new phase boundary is determined through

$$\Omega_c + 2G_2 - 2\rho\Sigma_{\zeta_-\zeta_-}(0) = 2k_0^2, \quad (14)$$

where $\Sigma_{\zeta_-\zeta_-}(0)$ should be evaluated at Ω_c . The solid lines in Fig. 6(d) show the relative phase transition shift as a function of k_0^2/G_1 for different G_2/G_1 . The shift becomes larger with decreasing k_0^2/G_1 and reaches its maximum at a critical spin-orbit coupling strength $k_{0,c}$, below which the plane wave phase is preempted by the stripe phase [42]. We plot the phase boundary shift for k_0 larger than the mean-field critical value $k_{0,c} = \sqrt{2G_2(1 + G_2/G_1)}$ [42]. It is possible that the mean-field critical spin-orbit coupling strength is shifted by quantum fluctuations, but this is beyond the scope of this paper and we expect that it does not change the results presented in Fig. 6(d) qualitatively. We also calculate the phase boundary by minimizing the ground-state energy $\mathcal{E}_{\text{mf}} + \mathcal{E}_{\text{LHY}}$. The technical details are given in Appendix C, and the phase boundary shifts obtained in this way are presented by the dots in Fig. 6(d). As can be seen, the two methods predict the same results. The self-energy $\Sigma_{\zeta_-\zeta_-}(0)$ also gives a correction to the spin polarizability,

$$\chi_M = \frac{2}{\Omega - \Omega_{c,\text{mf}} - 2\rho\Sigma_{\zeta_-\zeta_-}(0)}, \quad (15)$$

which diverges at the corrected phase boundary but becomes finite at the mean-field phase transition point. We have checked numerically that around Ω_c , the dependence of the self-energy $\Sigma_{\zeta_-\zeta_-}(0)$ on Ω is weak, and therefore χ_M diverges as $1/(\Omega - \Omega_c)$ close to the phase boundary, as predicted by the mean-field theory. The spin polarizability has been measured [20], and it seems that our one-loop result agrees better with the experimental data than the mean-field theory, see Fig. 7. However, the current experimental data cannot lead to a decisive conclusion and future experiments are required to verify our prediction.

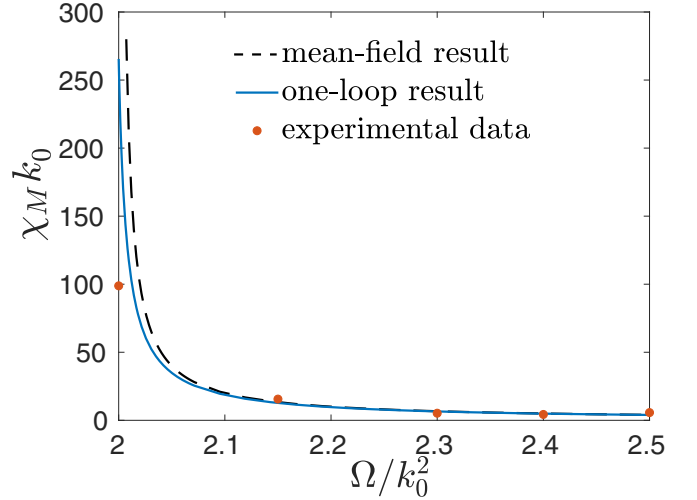


FIG. 7. The spin polarizability as a function of Ω . The experimental data are taken from Ref. [20]. To simulate the experiment, we use $k_0^2 = 4.2G_1$, $\sqrt{g_+^3\rho} = 0.2$, and $G_2/G_1 = 10^{-3}$ in the one-loop calculation.

D. Sound velocity and damping rate

Using the one-loop results for the static density response K^{-1} and the superfluid density ρ_x , we obtain the quantum corrected sound velocity in the x direction, $c_x = \sqrt{K^{-1}\rho_x}$. At the corrected phase transition point, the sound velocity c_x vanishes because of the vanishing superfluid density ρ_x . This is different from the result in Ref. [54], where a nonzero sound velocity at the phase boundary has been predicted within the Hartree-Fock-Bogoliubov-Popov approximation.

Since the sound velocity goes to zero slower than the superfluid density, it is easier to detect the beyond mean-field effects through the measurement of the sound velocity. In Fig. 8 we plot the c_x against $\sqrt{\delta\Omega}/k_0$, with $\delta\Omega = \Omega - \Omega_{c,\text{mf}}$. For typical experimental parameters [19–21], the one-loop prediction deviates clearly from the mean-field behavior when

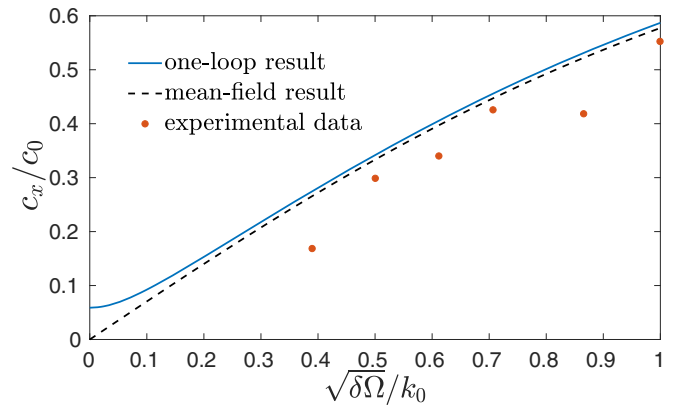


FIG. 8. The sound velocity c_x along the x direction ($c_0 = \sqrt{G_1}$). Here $\delta\Omega = \Omega - \Omega_{c,\text{mf}}$ is the deviation of Ω from the mean-field phase transition value. The experimental data are taken from Ref. [21], and the parameters we use to calculate the one-loop result are $k_0^2 = 5.2G_1$, $\sqrt{g_+^3\rho} = 0.18$, and $G_2/G_1 = 10^{-3}$, which correspond to the experiment in Ref. [21].

$\sqrt{\delta\Omega}/k_0 < 0.1$. The sound velocity has been measured [21], but the parameters are not close enough to the phase transition point. However, our prediction should be observable with current experimental methods.

Finally, we calculate the damping rate of phonons, for details see Appendix D. At zero temperature, the damping is due to the Beliaev process [55], i.e., an excitation decays into two with lower energy. In the small momentum limit ($q_y, q_z \ll \sqrt{G_1}$ and $q_x \ll \sqrt{\Omega - 2k_0^2}$), we find

$$\gamma_B = \frac{3q^5}{640\pi\rho} \left[1 - \frac{2\Omega k_0^2 \cos^2 \theta}{(\Omega + 2G_2)^2} \right]^2 \sqrt{1 + \frac{2k_0^2 \sin^2 \theta}{\Omega - \Omega_{c,\text{mf}}}}, \quad (16)$$

which coincides with the result obtained in Ref. [41]. The Beliaev damping is strongly suppressed along the direction of the spin-orbit coupling.

At finite temperature, the Landau damping [56] arises because the phonon couples to thermal excitations. The Landau damping is experimentally more relevant since it is responsible for damping in trapped Bose gases [57–59]. In the low-temperature and small-momentum limit ($c_\theta q \ll T \ll \Omega - 2k_0^2$), we obtain

$$\gamma_L = \frac{3\pi^3 q T^4}{40\rho c_\theta^4} \left[1 - \frac{2\Omega k_0^2 \cos^2 \theta}{(\Omega + 2G_2)^2} \right]^2 \sqrt{1 + \frac{2k_0^2 \sin^2 \theta}{\Omega - \Omega_{c,\text{mf}}}}. \quad (17)$$

Because of the extra c_θ dependence, the Landau damping rate, unlike the Beliaev decay, is not suppressed in the direction of spin-orbit coupling, which means that the Landau process is the dominant damping mechanism even for uniform systems at very low temperature.

V. CONCLUSIONS

We calculate systematically the one-loop corrections to a spin-orbit coupled Bose-Einstein condensate. We find that quantum fluctuations cause quantitative modifications to the superfluid density, spin polarizability, sound velocity, and damping rate. The quantum depletion increases while the LHY energy decreases with the transverse field in the zero momentum phase. The phase boundary between the plane wave and zero momentum phases is shifted to a smaller transverse field. The superfluid density vanishes and the spin polarizability diverges at the one-loop phase transition point. But at the mean-field phase boundary, the spin polarizability remains finite, consistent with an experimental measurement [20]. We also point out that the beyond mean-field corrections may be detected through the measurement of the sound velocity, and give the parameter regime in which the deviation from the mean-field behavior is visible. We calculate the Beliaev and Landau damping rates and identify the Landau damping

as the dominant mechanism of quasiparticle decay. Our results show that the spin-orbit coupling leads to, even for moderate interactions, quantum fluctuations strong enough to make detectable modifications to the properties of a macroscopic quantum state such as a Bose-Einstein condensate. The results can be readily tested in ultracold quantum gases, and in the future, in spin-orbit coupled Bose-Einstein condensates realized in other systems.

ACKNOWLEDGMENTS

This work was supported by the Academy of Finland under Projects No. 303351, No. 307419, and No. 318987; and by the European Research Council (Grant No. ERC-2013-AdG-340748-CODE). L.L. would like to acknowledge the Aalto Centre for Quantum Engineering for support.

APPENDIX A: MEAN-FIELD RESULTS

In this section we present the mean-field results of the excitation energy, density and spin response function, and superfluid density with some detailed derivations.

1. Excitation energy

The excitation energy is determined by $\det \mathcal{G}_0^{-1} = 0$, which gives

$$\varepsilon_{\text{ph}}^2(\mathbf{q}) = \frac{a(\mathbf{q}) - \sqrt{a^2(\mathbf{q}) - b(\mathbf{q})}}{2}, \quad (A1)$$

$$\varepsilon_{\text{sp}}^2(\mathbf{q}) = \frac{a(\mathbf{q}) + \sqrt{a^2(\mathbf{q}) - b(\mathbf{q})}}{2}, \quad (A2)$$

where $a(\mathbf{q}) = \mathcal{A}(\mathbf{q})\mathcal{B}(\mathbf{q}) + \mathcal{C}(\mathbf{q})\mathcal{D}(\mathbf{q}) + 2k_0^2 q_x^2$, $b(\mathbf{q}) = 4[\mathcal{A}(\mathbf{q})\mathcal{D}(\mathbf{q}) - k_0^2 q_x^2][\mathcal{B}(\mathbf{q})\mathcal{C}(\mathbf{q}) - k_0^2 q_x^2]$, ε_{ph} is the gapless phonon mode, and ε_{sp} is the gapped mode, which is dominated by spin excitations. In the small momentum limit,

$$\varepsilon_{\text{sp}} = \Delta_0 + \frac{q^2}{2m_{\text{sp}}}, \quad (A3)$$

$$\varepsilon_{\text{ph}} = c_\theta q + d_\theta q^3, \quad (A4)$$

where

$$\Delta_0 = \sqrt{\Omega(\Omega + 2G_2)}, \quad (A5)$$

$$m_{\text{sp}}^{-1} = \frac{(G_2 + \Omega)(2G_2 + \Omega) + 2k_0^2(\Omega + G_1 + 2G_2)\cos^2 \theta}{\sqrt{\Omega(2G_2 + \Omega)^{3/2}}}, \quad (A6)$$

$$c_\theta = c_0 \sqrt{1 - \frac{2k_0^2 \cos^2 \theta}{\Omega + 2G_2}}, \quad (A7)$$

$$d_\theta = \frac{1}{8c_\theta} \left(1 - \frac{4k_0^2 [(\Omega + 2G_2)(\Omega^2 + (G_1 + 3G_2)\Omega + 2(G_1 + G_2)^2)\cos^2 \theta - k_0^2(\Omega + 2(G_1 + G_2))^2 \cos^4 \theta]}{\Omega(\Omega + 2G_2)^3} \right), \quad (A8)$$

with $c_0 = \sqrt{G_1}$ being the usual Bogoliubov sound velocity for a weakly interacting single component Bose-Einstein condensate. In the absence of spin-orbit coupling, the sound velocity is the same as c_0 . In the presence of spin-orbit coupling, it depends on θ , which is the angle between the momentum \mathbf{q} and direction of the spin-orbit coupling. When $\Omega = 2k_0^2 - 2G_2$, the sound

velocity along the x direction becomes zero, and the phonon dispersion along the x direction becomes quadratic,

$$\varepsilon_{\text{ph}} = \sqrt{G_1 q_{\parallel}^2 + \frac{1}{4} q_{\parallel}^4 + \frac{G_2 q_x^4}{4G_2 + 2\Omega} - \frac{(G_1 + G_2)[2(G_1 + G_2) + \Omega]}{2\Omega(2G_2 + \Omega)} q_{\parallel}^2 q_x^2}, \quad (\text{A9})$$

with $q_{\parallel}^2 = q_y^2 + q_z^2$.

Knowing the low-energy dispersion relation of the phonons, we can define the momentum region in which the dispersion is linear. When the momentum is along the x direction, by requiring $c_x q_x \gg d_x q_x^3$, we find the condition

$$q_x \ll \sqrt{\Omega - 2k_0^2}. \quad (\text{A10})$$

When the momentum is along the y or z direction, the condition is

$$q_y, q_z \ll \sqrt{G_1}. \quad (\text{A11})$$

At finite temperature, the linear dispersion region also requires that the dispersion of the thermal excitations is linear, and this leads to the condition

$$T \ll \Omega - 2k_0^2. \quad (\text{A12})$$

These conditions are used in deriving the analytical expressions for Beliaev and Landau damping rates.

2. Density and spin response functions

In the modulus-phase representation, the density and spin response functions are given by the Green's functions $\mathcal{G}_{\zeta_+\zeta_+}$ and $\mathcal{G}_{\zeta_-\zeta_-}$, respectively. So the spin polarizability defined in Refs. [48,49] is simply given by $\mathcal{G}_{\zeta_-\zeta_-}(q_x \rightarrow 0)/\rho$, and at the mean-field level,

$$\chi_M = \mathcal{G}_{0,\zeta_-\zeta_-}(q_x \rightarrow 0)/\rho = \frac{2}{\Omega + 2G_2 - 2k_0^2}. \quad (\text{A13})$$

The mean-field density and spin static structure factors are given by

$$\begin{aligned} S_d(\mathbf{q}) &= \int d\omega \mathcal{G}_{0,\zeta_+\zeta_+}(\omega, \mathbf{q})/\rho, \quad S_s(\mathbf{q}) \\ &= \int d\omega \mathcal{G}_{0,\zeta_-\zeta_-}(\omega, \mathbf{q})/\rho. \end{aligned} \quad (\text{A14})$$

We show the mean-field static structure factors for different spin-orbit coupling strength in Fig. 9. As comparison, the contribution of the phonon branch are also shown. Without spin-orbit coupling, the density and spin excitations are decoupled and the phonon branch does not contribute to the spin structure factor. In the presence of spin-orbit coupling, a density perturbation along the x direction also induces a spin response and vice versa, so the density and spin structure factors are carried by both the phonon and gapped excitations. In the large momentum limit, the total static structure factors approach to 1 and the phonon branch contributes to one half. Remarkably, we find a peak in the total spin static structure factor. When the parameter approaches to the phase transition point, the peak becomes higher and its location moves to the zero momentum. By contrast, the peak is not observed in the total density structure factor, although there is peak in the contribution of the phonon branch.

3. Superfluid density

To get the superfluid density, we integrate out the φ and ζ_- fields and obtain an effective theory of ϕ and ζ_+

$$\mathcal{L}_{\text{eff}} = \frac{1}{2} [\phi, \zeta_+] \mathcal{G}_{0,\text{eff}}^{-1} [\phi, \zeta_+]^T, \quad (\text{A15})$$

where

$$\begin{aligned} \mathcal{G}_{0,\text{eff}}^{-1} &= \begin{bmatrix} \rho \mathbf{q}^2 & -\omega_n \\ \omega_n & \frac{\mathbf{q}^2}{4\rho} + g_+ \end{bmatrix} - \begin{bmatrix} 0 & ik_0 q_x \\ -ik_0 q_x & 0 \end{bmatrix} \\ &\times \begin{bmatrix} \rho \mathbf{q}^2 + 2\Omega\rho & -\omega_n \\ \omega_n & \frac{\mathbf{q}^2}{4\rho} + g_- + \frac{\Omega}{2\rho} \end{bmatrix}^{-1} \begin{bmatrix} 0 & ik_0 q_x \\ -ik_0 q_x & 0 \end{bmatrix}, \end{aligned} \quad (\text{A16})$$

which in the low-energy limit is

$$\mathcal{G}_{0,\text{eff}}^{-1} = \begin{bmatrix} \rho(\mathbf{q}^2 - \frac{2k_0^2}{\Omega + 2G_2} q_x^2) & -\omega_n \\ \omega_n & \frac{\mathbf{q}^2}{4\rho} + g_+ \end{bmatrix}. \quad (\text{A17})$$

Integrating out the ζ_+ field, we arrive at an effective Lagrangian of the phase fluctuation, and in the low-energy and long-wavelength limit,

$$\mathcal{L}_{\text{eff}} = (K^{-1} \omega_n^2 + \rho_i q_i^2) |\phi|^2, \quad (\text{A18})$$

where K is the zero momentum static density response function whose mean-field value is $1/g_+$, and the mean-field superfluid densities are

$$\rho_x = \rho \left(1 - \frac{2k_0^2}{\Omega + 2G_2} \right), \quad \rho_y = \rho_z = \rho. \quad (\text{A19})$$

APPENDIX B: ANALYTICAL RESULTS OF ONE-LOOP CORRECTIONS IN THE ABSENCE OF SPIN-ORBIT COUPLING

Without the spin-orbit coupling, we can calculate the one-loop corrections analytically. It is useful to calculate the

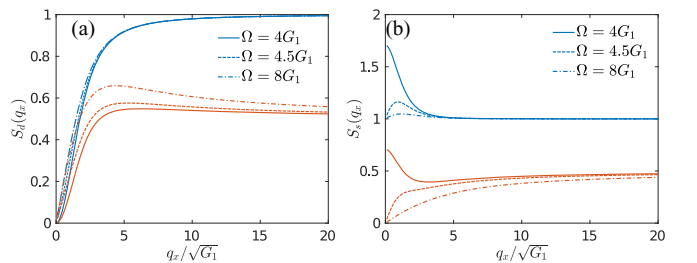


FIG. 9. The (a) density and (b) spin static structure factors (blue upper lines). Both approach unity in the large momentum limit. The contribution of the phonon branch are also shown (red lower lines). The interaction is taken to be $SU(2)$ invariant with $G_2 = 0$ and G_1 is taken to be unit. There is a peak in the spin structure factor.

following integral,

$$I(\alpha, m^2; \beta, M^2; \gamma) = \int \frac{d^d k}{(2\pi)^d} \frac{k^\gamma}{(k^2 + m^2)^\alpha (k^2 + M^2)^\beta} = \frac{2\pi^{d/2}}{(2\pi)^d \Gamma(d/2)} \frac{k^{d-1+\gamma}}{(k^2 + m^2)^\alpha (k^2 + M^2)^\beta}, \quad (\text{B1})$$

$$= \frac{2\pi^{d/2}}{(2\pi)^d \Gamma(d/2)} \frac{\Gamma(\alpha + \beta)}{\Gamma(\alpha)\Gamma(\beta)} \int_0^1 dx \frac{k^{d-1+\gamma} x^{\alpha-1} (1-x)^{\beta-1}}{[x(k^2 + m^2) + (1-x)(k^2 + M^2)]^{\alpha+\beta}}, \quad (\text{B2})$$

$$= \frac{2\pi^{d/2}}{(2\pi)^d \Gamma(d/2)} \frac{(M^2)^{\frac{d+\gamma}{2}-\alpha-\beta}}{\Gamma(\alpha + \beta)} \Gamma\left(\alpha + \beta - \frac{d+\gamma}{2}\right) \Gamma\left(\frac{d+\gamma}{2}\right) {}_2F_1\left(\alpha, \alpha + \beta - \frac{d+\gamma}{2}; \alpha + \beta; 1 - \frac{m^2}{M^2}\right), \quad (\text{B3})$$

where ${}_2F_1(a, b; c; z)$ is the hypergeometric function. To get the above result we have used dimensional regularization.

The condensate fraction is

$$|\langle \psi_\uparrow \rangle|^2 + |\langle \psi_\downarrow \rangle|^2 = \frac{1}{2} (|\langle \sqrt{\rho} + \zeta_1 e^{i(\phi+\varphi)} \rangle|^2 + |\langle -\sqrt{\rho} + \zeta_2 e^{i(\phi-\varphi)} \rangle|^2) \approx \rho - \frac{1}{4\rho} (\langle \zeta_+^2 \rangle + \langle \zeta_-^2 \rangle) - \rho (\langle \varphi^2 \rangle + \langle \phi^2 \rangle), \quad (\text{B4})$$

so the quantum depletion is

$$\delta\rho = \frac{1}{4\rho} (\langle \zeta_+^2 \rangle + \langle \zeta_-^2 \rangle) + \rho (\langle \varphi^2 \rangle + \langle \phi^2 \rangle) = \frac{(g_+\rho)^{3/2}}{3\pi^2} + \frac{(g_-\rho)^{3/2}}{3\pi^2} \sqrt{1+x/2} \left[(x+1)E\left(\frac{2}{x+2}\right) - xK\left(\frac{2}{x+2}\right) \right], \quad (\text{B5})$$

with $x = \Omega/(g_-\rho)$ and $E(z)$ and $K(z)$ are the complete elliptic integral of the second and first kind, respectively. The quantum depletion increases with increasing g_+ and g_- , but decreases with increasing Ω .

The transverse spin polarization is

$$\langle \sigma_x \rangle = \frac{1}{\rho} \langle \psi^\dagger \sigma_x \psi \rangle \approx -1 + 2\langle \varphi^2 \rangle + \frac{1}{2\rho^2} \langle \zeta_-^2 \rangle, \quad (\text{B6})$$

so

$$\delta\langle \sigma_x \rangle = 2\langle \varphi^2 \rangle + \frac{1}{2\rho^2} \langle \zeta_-^2 \rangle = \frac{2(g_-\rho)^{3/2}}{3\rho\pi^2} \sqrt{1+x/2} \left[(x+1)E\left(\frac{2}{x+2}\right) - xK\left(\frac{2}{x+2}\right) \right]. \quad (\text{B7})$$

The Lee-Huang-Yang correction [51] can be obtained as the zero point energy of the system [52], and we find

$$\mathcal{E}_{\text{LHY}} = \frac{8}{15\pi^2} g_+ \rho^2 \sqrt{g_+^3 \rho} + \frac{(g_-\rho)^{5/2} \sqrt{1+x/2}}{4\pi} {}_2F_1\left(-\frac{1}{2}, \frac{3}{2}; 3; \frac{2}{2+x}\right). \quad (\text{B8})$$

The first term in Eq. (B8) is the same as the result for a weakly-interacting spinless Bose gas [51]. The second term comes from the spin excitation. The function ${}_2F_1(-\frac{1}{2}, \frac{3}{2}; 3; \frac{2}{2+x})$ depends weakly on x , with ${}_2F_1(-\frac{1}{2}, \frac{3}{2}; 3; 1) = 32/(15\pi)$ and ${}_2F_1(-\frac{1}{2}, \frac{3}{2}; 3; 0) = 1$, so the second term increases with increasing g_- and Ω .

The chemical potential shift is given by the tadpole diagrams shown in Fig. 5. Evaluating the integrals, we find

$$\delta\mu = \frac{4g_+\rho \sqrt{g_+^3 \rho}}{3\pi^2} + \frac{g_-\rho \sqrt{g_-^3 \rho} \sqrt{1+x/2}}{3\pi^2} \left[(4+x)E\left(\frac{2}{2+x}\right) - xK\left(\frac{2}{2+x}\right) \right], \quad (\text{B9})$$

which increases with g_+ , g_- , and Ω . Another way to calculate the chemical potential shift is to take derivative of the LHY energy density \mathcal{E}_{LHY} with respect to ρ , $\delta\mu = \partial_\rho \mathcal{E}_{\text{LHY}}$, and the result is the same as Eq. (B9).

The correction to K^{-1} is given by $\Sigma_{\zeta_+\zeta_+}(0)$, and in the absence of spin-orbit coupling,

$$\delta K^{-1} = -\Sigma_{\zeta_+\zeta_+}(0) = \frac{2g_+ \sqrt{g_+^3 \rho}}{\pi^2} + \frac{g_- \sqrt{g_-^3 \rho} \sqrt{1+x/2}}{2\pi} {}_2F_1\left(-\frac{1}{2}, -\frac{1}{2}; 1; \frac{2}{2+x}\right). \quad (\text{B10})$$

Note that δK^{-1} can be related to $\delta\mu$ through $\delta K^{-1} = \partial_\rho \delta\mu$.

To calculate the correction to the mean-field excitation gap Δ_0 , we need to compute the self-energies $\Sigma_{\varphi\varphi}(\Delta_0)$, $\Sigma_{\zeta_-\zeta_-}(\Delta_0)$, and $\Sigma_{\varphi\zeta_-}(\Delta_0)$, which can also be done analytically in the absence of the spin-orbit coupling, and we find that the one-loop correction to the gap is zero. In the presence of spin-orbit coupling, we calculate the self-energies numerically, and find the one-loop correction increases the gap slightly, see the main text.

APPENDIX C: PHASE BOUNDARY BETWEEN THE PLANE WAVE AND ZERO MOMENTUM PHASES: THE EFFECT OF THE LHY ENERGY

In this section we study the phase boundary between the zero momentum and plane wave phases by minimizing the ground state energy. As we will show, this also provides another way to calculate the superfluid density.

We only consider the plane wave and zero momentum phases, and in general the field operator can be written as

$$\psi = e^{i\phi + ik_1 x} \begin{bmatrix} \sqrt{\rho + \zeta_1} \cos \alpha e^{i\varphi} \\ -\sqrt{\rho + \zeta_2} \sin \alpha e^{-i\varphi} \end{bmatrix}, \quad (\text{C1})$$

where we have introduced the phase fluctuations ϕ and φ , and the density fluctuations ζ_1 and ζ_2 , which are simply set to be zero in the mean-field approximation. The parameters k_1 and α should be determined by minimizing the ground-state energy, and $k_1 \neq 0$ characterizes the plane wave phase while $k_1 = 0$ gives the zero momentum phase.

Substituting Eq. (C1) to the Lagrangian density

$$\mathcal{L} = \psi^\dagger (\partial_\tau + h_0 - \mu) \psi + \frac{g_+}{2} (\psi^\dagger \psi)^2 + \frac{g_-}{2} (\psi^\dagger \sigma_z \psi)^2, \quad (\text{C2})$$

and up to the quadratic order of the fluctuations, we find

$$\begin{aligned} \mathcal{L} = & \frac{k_1^2 + k_0^2}{2} \rho - k_0 k_1 \rho \cos 2\alpha - \frac{\Omega}{2} \rho \sin 2\alpha + \frac{g_+ + g_- \cos^2 2\alpha}{2} \rho^2 - \mu \rho \\ & + \left(\frac{k_1^2 + k_0^2}{2} - \frac{\Omega}{2 \sin 2\alpha} + G_1 - \mu \right) \zeta_+ + \left(\frac{\Omega \cos 2\alpha}{2 \sin 2\alpha} - k_0 k_1 + G_2 \cos 2\alpha \right) \zeta_- \\ & + \frac{1}{2} [\phi, \zeta_+, \varphi, \zeta_-] \mathcal{G}_0^{-1} [\phi, \zeta_+, \varphi, \zeta_-]^T, \end{aligned} \quad (\text{C3})$$

where $\zeta_+ = \zeta_1 \cos^2 \alpha + \zeta_2 \sin^2 \alpha$, $\zeta_- = \zeta_1 \cos^2 \alpha - \zeta_2 \sin^2 \alpha$, and \mathcal{G}_0^{-1} in the momentum and frequency representation reads

$$\mathcal{G}_0^{-1}(i\omega, \mathbf{k}) = \begin{bmatrix} \rho k^2 & -\omega - ik_1 k_x & \rho k^2 \cos 2\alpha & ik_0 k_x \\ \omega + ik_1 k_x & \frac{k^2}{4\rho \sin^2 2\alpha} + g_+ + \frac{\cos^2 2\alpha}{2 \sin^2 2\alpha} \frac{\Omega}{\rho} & -ik_0 k_x & -\frac{\Omega \cos 2\alpha}{2\rho \sin^2 2\alpha} - \frac{\cos 2\alpha}{4\rho \sin^2 2\alpha} k^2 \\ \rho k^2 \cos 2\alpha & ik_0 k_x & \rho k^2 + 2\Omega \rho \sin 2\alpha & -\omega - ik_1 k_x \\ -ik_0 k_x & -\frac{\Omega \cos 2\alpha}{2\rho \sin^2 2\alpha} - \frac{\cos 2\alpha}{4\rho \sin^2 2\alpha} k^2 & \omega + ik_1 k_x & \frac{k^2}{4\rho \sin^2 2\alpha} + g_- + \frac{1}{2 \sin^2 2\alpha} \frac{\Omega}{\rho} \end{bmatrix}. \quad (\text{C4})$$

We choose the renormalization condition $\langle \zeta_+ \rangle = \langle \zeta_- \rangle = 0$, which gives two conditions at the mean-field level

$$\frac{k_1^2 + k_0^2}{2} - \frac{\Omega}{2 \sin 2\alpha} + G_1 - \mu = 0, \quad (\text{C5})$$

$$\frac{\Omega \cos 2\alpha}{2 \sin 2\alpha} - k_0 k_1 + G_2 \cos 2\alpha = 0. \quad (\text{C6})$$

The first condition Eq. (C5) determines the mean-field chemical potential and the second condition Eq. (C6) gives a relation between α and k_1 . Note that for small k_1 , we have $\cos 2\alpha \propto k_1$.

The mean-field energy density is given by the first line in Eq. (C3),

$$\begin{aligned} \mathcal{E}_{\text{mf}} = & \frac{k_1^2 + k_0^2}{2} \rho - k_0 k_1 \rho \cos 2\alpha - \frac{\Omega}{2} \rho \sin 2\alpha \\ & + \frac{g_+ + g_- \cos^2 2\alpha}{2} \rho^2. \end{aligned} \quad (\text{C7})$$

Note that Eq. (C6) can also be obtained by minimizing the energy with respect to α . In Ref. [42], a relation between k_1 and α is obtained by minimizing the energy with respect to k_1 , which leads to $\alpha = \arccos(k_1/k_0)/2$. This relation and Eq. (C6) determine the mean-field value of α and k_1 and therefore the mean-field phase boundary, which are the same as the results in Ref. [42]. However, $\alpha = \arccos(k_1/k_0)/2$ no longer holds when the LHY energy is taken into account because in this case there will be extra contribution to the energy density depending on k_1 . In contrast, Eq. (C6) is

still valid up to at least one loop since there is no one-loop correction proportional to ζ_- and therefore $\langle \zeta_- \rangle = 0$ leads to the same condition. Therefore, to include the effects of the LHY energy, we should utilize the condition Eq. (C6) instead of the form used in Ref. [42].

Using Eq. (C6), we can rewrite \mathcal{E}_{mf} in terms of k_1 , and then we can view the resultant expression as a Landau functional in terms of the order parameter k_1 . The disordered phase corresponds to the zero momentum phase while the ordered phase is the plane wave phase. Technically, it is simpler to use $x \equiv \cos 2\alpha$ as the order parameter (because $x \propto k_1$ for small k_1) and we have

$$\begin{aligned} \mathcal{E}_{\text{mf}} = & \frac{k_0^2}{2} \rho - \frac{\Omega}{2\sqrt{1-x^2}} \rho + \frac{g_+ \rho^2}{2} \\ & + \frac{\rho}{2k_0^2} \left[\frac{\Omega x}{2\sqrt{1-x^2}} + g_- \rho x \right]^2 - \frac{g_- \rho^2 x^2}{2}. \end{aligned} \quad (\text{C8})$$

By minimizing the above express with respect to x , we can determine the mean-field phase diagram.

Expanding Eq. (C8) around $x = 0$ and rewriting the result in terms of k_1 , we get

$$\mathcal{E}_{\text{mf}} = \frac{k_0^2}{2}\rho - \frac{\Omega}{2}\rho + \frac{g+\rho^2}{2} + \frac{\rho}{2}\left[1 - \frac{2k_0^2}{\Omega + 2G_2}\right]k_1^2. \quad (\text{C9})$$

It is then clear that the mean-field phase transition point is determined by $1 - \frac{2k_0^2}{\Omega + 2G_2} = 0$. In the zero momentum phase, the coefficient before k_1 measures the energy cost of the phase fluctuations, and therefore it is by definition the superfluid density $\rho_x/2$. From the point view of the Landau theory of phase transitions, the superfluid density is the coefficient of the quadratic term in the order parameter expansion. A negative superfluid density simply means that the zero momentum phase is unstable, and k_1 will acquire a nonzero expectation value such that the system enters the plane wave phase. In the plane wave phase, the superfluid density becomes positive again.

To calculate the correction to the mean-field phase boundary, we include the LHY contribution to the ground-state energy density and minimize $\mathcal{E}_{\text{mf}} + \mathcal{E}_{\text{LHY}}$ as a function of k_1 . The LHY energy is obtained through the excitation energy determined by $\det \mathcal{G}_0^{-1} = 0$ with \mathcal{G}_0^{-1} given by Eq. (C4). The minimization can be done in the following way: We first calculate numerically the LHY energy for small k_1 , and then extract the coefficient of the k_1^2 term in \mathcal{E}_{LHY} . This coefficient gives a correction to the coefficient of k_1^2 in Eq. (C9), and the new phase boundary is determined by requiring the corrected coefficient to be zero. As shown in Fig. 6(d), the phase boundary determined in this way agrees perfectly with the one determined through the one-loop result of ρ_x .

Before closing this section, we mention that the same method can be used to get the superfluid density in the plane wave phase. Assuming \mathcal{E}_{mf} reaches its minimal at $k_{1,c}$, then the superfluid density is obtained by expanding the mean-field energy Eq. (C8) around $k_{1,c}$,

$$\mathcal{E}_{\text{mf}} = \mathcal{E}_{\text{mf}}(k_{1,c}) + \frac{\rho_x}{2}\delta k^2, \quad (\text{C10})$$

where $\delta k = k_1 - k_{1,c}$. To find $k_{1,c}$ we minimize Eq. (C8) with respect to x and find the position x_c at which the energy takes minimum. Then using Eq. (C6), we find $k_{1,c} = k_0\sqrt{1 - \Omega^2/\Omega_{c,\text{mf}}^2}$. Expanding Eq. (C8) around x_c and change the variable from $x - x_c$ to $k_1 - k_{1,c}$, we obtain the mean-field superfluid density in the plane wave phase

$$\rho_x = \rho - \rho \frac{k_0^2 \Omega^2}{\Omega^2 G_2 + 4(k_0^2 - G_2)^3}, \quad (\text{C11})$$

which is the same as the result in Ref. [50]. By taking into account the LHY contribution, we can also obtain the correction to the mean-field superfluid density in the plane wave phase.

APPENDIX D: DAMPING RATE AT ZERO AND FINITE TEMPERATURE

The damping rate γ , i.e., the imaginary part of the phonon excitation energy, is determined by

$$\det [G_0^{-1}(\varepsilon_{\text{ph}} - i\gamma, \mathbf{q}) - \Sigma(\varepsilon_{\text{ph}} + i0^+, \mathbf{q})] = 0, \quad (\text{D1})$$



FIG. 10. Feynman diagrams for $\Sigma_{\phi\phi}$ that contribute to the phonon damping rates.

where $\Sigma(\varepsilon_{\text{ph}} + i0^+, \mathbf{q})$ is the one-loop self-energy evaluated at the phonon frequency.

To solve Eq. (D1), we first integrate out the φ and ζ_- fields and obtain an effective theory for the low-energy mode [c.f. Eq. (A15)]

$$\mathcal{L}_{\text{eff}} = \frac{1}{2}[\phi, \zeta_+] \mathcal{G}_{\text{eff}}^{-1}[\phi, \zeta_+]^T, \quad (\text{D2})$$

where $\mathcal{G}_{\text{eff}}^{-1}$ can be written as

$$\mathcal{G}_{\text{eff}}^{-1} = \begin{bmatrix} \rho(\mathbf{q}^2 - \frac{2k_0^2}{\Omega + 2G_2} q_x^2) & -\omega_n \\ \omega_n & \frac{\mathbf{q}^2}{4\rho} + g_+ \end{bmatrix} - \begin{bmatrix} \Im \Sigma_{\text{eff},\phi\phi} & \Im \Sigma_{\text{eff},\phi\zeta_+} \\ \Im \Sigma_{\text{eff},\zeta_+\phi} & \Im \Sigma_{\text{eff},\zeta_+\zeta_+} \end{bmatrix}. \quad (\text{D3})$$

And then from Eq. (D3), the damping rate is obtained

$$\gamma = \frac{\rho(\mathbf{q}^2 - \frac{2k_0^2}{\Omega + 2G_2} q_x^2) \Im \Sigma_{\text{eff},\zeta_+\zeta_+} + g_+ \Im \Sigma_{\text{eff},\phi\phi}}{2\varepsilon_{\text{ph}}} + \Im \Sigma_{\text{eff},\phi\zeta_+}. \quad (\text{D4})$$

We focus on the linear dispersion regime defined through Eqs. (A10)–(A12). By analyzing the low-energy and momentum behavior of all the one-loop self-energies, we find that it is enough to consider the Feynman diagrams constructed from only two vertices Figs. 2(a) and 2(d), and the momentum dependence of vertex Fig. 2(d) can be neglected. Therefore the relevant parts of the effective self-energy matrix is

$$\begin{bmatrix} \Im \Sigma_{\text{eff},\phi\phi} & \Im \Sigma_{\text{eff},\phi\zeta_+} \\ \Im \Sigma_{\text{eff},\zeta_+\phi} & \Im \Sigma_{\text{eff},\zeta_+\zeta_+} \end{bmatrix} = \begin{bmatrix} \Im \Sigma_{\phi\phi} & \Im \Sigma_{\phi\zeta_+} \\ \Im \Sigma_{\zeta_+\phi} & \Im \Sigma_{\zeta_+\zeta_+} \end{bmatrix} + \begin{bmatrix} -\frac{4\rho k_0 q_x \Im \Sigma_{\phi\zeta_-}}{\Omega + 2G_2} + \frac{4\rho^2 k_0^2 q_x^2 \Im \Sigma_{\zeta_-\zeta_-}}{(\Omega + 2G_2)^2} & -\frac{2\rho k_0 q_x \Im \Sigma_{\zeta_+\zeta_-}}{\Omega + 2G_2} \\ \frac{2\rho k_0 q_x \Im \Sigma_{\zeta_+\zeta_-}}{\Omega + 2G_2} & 0 \end{bmatrix}. \quad (\text{D5})$$

As an example, we calculate $\Sigma_{\phi\phi}(i\omega_n, \mathbf{q})$ explicitly. The Feynman diagrams are shown in Fig. 10.

$$\begin{aligned} \Sigma_{\phi\phi}(i\omega_n, \mathbf{q}) &= \sum_{\omega'_m, \mathbf{k}} [(\mathbf{k} \cdot \mathbf{q})^2 \mathcal{G}_{0,\phi\phi}(i\omega'_m, \mathbf{k}) \mathcal{G}_{0,\zeta_+\zeta_+}(i\omega_n - i\omega'_m, \mathbf{q} - \mathbf{k}) \\ &\quad + \mathbf{k} \cdot \mathbf{q} (\mathbf{q}^2 - \mathbf{k} \cdot \mathbf{q}) \mathcal{G}_{0,\phi\zeta_+}(i\omega'_m, \mathbf{k}) \mathcal{G}_{0,\phi\zeta_+}(i\omega_n - i\omega'_m, \mathbf{q} - \mathbf{k})]. \end{aligned} \quad (\text{D6})$$

We write the mean-field Green's function explicitly

$$\mathcal{G}_{0,\phi\phi}(i\omega_n, \mathbf{q}) = \frac{A_{11}(\mathbf{q})}{\omega_n^2 + \varepsilon_{\text{sp}}^2(\mathbf{q})} + \frac{B_{11}(\mathbf{q})}{\omega_n^2 + \varepsilon_{\text{ph}}^2(\mathbf{q})}, \quad (\text{D7})$$

$$\mathcal{G}_{0,\zeta+\zeta+}(i\omega_n, \mathbf{q}) = \frac{A_{22}(\mathbf{q})}{\omega_n^2 + \varepsilon_{\text{sp}}^2(\mathbf{q})} + \frac{B_{22}(\mathbf{q})}{\omega_n^2 + \varepsilon_{\text{ph}}^2(\mathbf{q})}, \quad (\text{D8})$$

$$\mathcal{G}_{0,\phi\zeta+}(i\omega_n, \mathbf{q}) = -\mathcal{G}_{0,\zeta+\phi}(i\omega_n, \mathbf{q}) = \frac{\omega A_{12}(\mathbf{q})}{\omega_n^2 + \varepsilon_{\text{sp}}^2(\mathbf{q})} + \frac{\omega B_{12}(\mathbf{q})}{\omega_n^2 + \varepsilon_{\text{ph}}^2(\mathbf{q})}. \quad (\text{D9})$$

Since we are studying the damping rate in the linear regime, the gapped branch can be neglected, and it is enough to know the low momentum behavior of B_{11} , B_{22} , and B_{12} ,

$$B_{11}(\mathbf{q}) \approx g_+, \quad B_{22}(\mathbf{q}) \approx \rho \frac{c_\theta^2}{c_0^2} \mathbf{q}^2, \quad B_{12}(\mathbf{q}) \approx 1. \quad (\text{D10})$$

Evaluating the Matsubara frequency summation, $\Sigma_{\phi\phi}(i\omega_n, \mathbf{q})$ can be written as

$$\Sigma_{\phi\phi}(i\omega_n, \mathbf{q}) = \Sigma_{\phi\phi,1}(i\omega_n, \mathbf{q}) + \Sigma_{\phi\phi,2}(i\omega_n, \mathbf{q}), \quad (\text{D11})$$

with

$$\begin{aligned} \Sigma_{\phi\phi,1}(i\omega_n, \mathbf{q}) &= \sum_{\mathbf{k}} [1 + n(\varepsilon_{\text{ph}}(\mathbf{k})) + n(\varepsilon_{\text{ph}}(\mathbf{q} - \mathbf{k}))] \left[\frac{1}{-i\omega_n + \varepsilon_{\text{ph}}(\mathbf{k}) + \varepsilon_{\text{ph}}(\mathbf{q} - \mathbf{k})} + \frac{1}{i\omega_n + \varepsilon_{\text{ph}}(\mathbf{k}) + \varepsilon_{\text{ph}}(\mathbf{q} - \mathbf{k})} \right] \\ &\times \left[(\mathbf{k} \cdot \mathbf{q})^2 \frac{B_{11}(\mathbf{k})B_{22}(\mathbf{q} - \mathbf{k})}{4\varepsilon_{\text{ph}}(\mathbf{k})\varepsilon_{\text{ph}}(\mathbf{q} - \mathbf{k})} + \mathbf{k} \cdot \mathbf{q} (\mathbf{q}^2 - \mathbf{k} \cdot \mathbf{q}) \frac{B_{12}(\mathbf{k})B_{12}(\mathbf{q} - \mathbf{k})}{4} \right], \end{aligned} \quad (\text{D12})$$

which is nonzero even if the temperature is zero and is relevant to the Beliaev damping rate, and

$$\begin{aligned} \Sigma_{\phi\phi,2}(i\omega_n, \mathbf{q}) &= \sum_{\mathbf{k}} [n(\varepsilon_{\text{ph}}(\mathbf{k})) - n(\varepsilon_{\text{ph}}(\mathbf{q} - \mathbf{k}))] \left[\frac{1}{i\omega_n + \varepsilon_{\text{ph}}(\mathbf{q} - \mathbf{k}) - \varepsilon_{\text{ph}}(\mathbf{k})} - \frac{1}{i\omega_n + \varepsilon_{\text{ph}}(\mathbf{k}) - \varepsilon_{\text{ph}}(\mathbf{q} - \mathbf{k})} \right] \\ &\times \left[(\mathbf{k} \cdot \mathbf{q})^2 \frac{B_{11}(\mathbf{k})B_{22}(\mathbf{q} - \mathbf{k})}{4\varepsilon_{\text{ph}}(\mathbf{k})\varepsilon_{\text{ph}}(\mathbf{q} - \mathbf{k})} - \mathbf{k} \cdot \mathbf{q} (\mathbf{q}^2 - \mathbf{k} \cdot \mathbf{q}) \frac{B_{12}(\mathbf{k})B_{12}(\mathbf{q} - \mathbf{k})}{4} \right], \end{aligned} \quad (\text{D13})$$

which is nonzero only at finite temperature and is relevant to the Landau damping rate.

We calculate the imaginary part of $\Sigma_{\phi\phi,1}(\varepsilon_{\text{ph}}(\mathbf{q}) + i0^+, \mathbf{q})$ at zero temperature,

$$\Im \Sigma_{\phi\phi,1}(\varepsilon_{\text{ph}}(\mathbf{q}) + i0^+, \mathbf{q}) = \pi \sum_{\mathbf{k}} \delta(-\varepsilon_{\text{ph}}(\mathbf{q}) + \varepsilon_{\text{ph}}(\mathbf{k}) + \varepsilon_{\text{ph}}(\mathbf{q} - \mathbf{k})) f(\mathbf{q}, \mathbf{k}), \quad (\text{D14})$$

$$f(\mathbf{q}, \mathbf{k}) = (\mathbf{k} \cdot \mathbf{q})^2 \frac{B_{11}(\mathbf{k})B_{22}(\mathbf{q} - \mathbf{k})}{4\varepsilon_{\text{ph}}(\mathbf{k})\varepsilon_{\text{ph}}(\mathbf{q} - \mathbf{k})} + \mathbf{k} \cdot \mathbf{q} (\mathbf{q}^2 - \mathbf{k} \cdot \mathbf{q}) \frac{B_{12}(\mathbf{k})B_{12}(\mathbf{q} - \mathbf{k})}{4}. \quad (\text{D15})$$

To calculate the above integral, we need to solve the internal \mathbf{k} allowed by the energy and momentum conservation. We can scale the momentum as $c_x k_x \equiv c_0 k'_x$ and $k_{y/z} = k'_{y/z}$, and then the phonon dispersion can be written as

$$\varepsilon_{\text{ph}}(\mathbf{k}) = \sqrt{c_x^2 k_x^2 + c_0 k_y^2 + c_0^2 k_z^2} = c_\theta k = c_0 k'. \quad (\text{D16})$$

The momentum and energy conservation can be solved in terms of the new variables in the small \mathbf{q} limit (θ' is the angle between \mathbf{k}' and \mathbf{q}'),

$$\delta(-c_0 q' + c_0 k' + c_0 |\mathbf{q}' - \mathbf{k}'|) = \frac{q' - k'}{c_0 q' k' \sin \theta'} \delta(\theta'), \quad (\text{D17})$$

with the restriction $k' < q'$. This means that \mathbf{k}' and \mathbf{q}' are along the same direction and $k' < q'$ and therefore \mathbf{k} and \mathbf{q} are also along the same direction and $k < q$. Under this condition,

$$f(\mathbf{q}, \mathbf{k}) = \frac{k q^2 (q - k)}{2}, \quad (\text{D18})$$

so

$$\Im \Sigma_{\phi\phi,1}(\varepsilon_{\text{ph}}(\mathbf{q}) + i0^+, \mathbf{q}) = \pi \int \frac{dk_x dk_y dk_z}{(2\pi)^3} f(\mathbf{q}, \mathbf{k}) \delta(-\varepsilon_{\text{ph}}(\mathbf{q}) + \varepsilon_{\text{ph}}(\mathbf{k}) + \varepsilon_{\text{ph}}(\mathbf{q} - \mathbf{k})), \quad (\text{D19})$$

$$= \pi \frac{c_0}{c_x} \int \frac{dk'_x dk'_y dk'_z}{(2\pi)^3} f(\mathbf{q}, \mathbf{k}) \delta(-c_0 q' + c_0 k' + c_0 |\mathbf{q}' - \mathbf{k}'|), \quad (\text{D20})$$

$$= \pi \frac{c_0}{c_x} \int \frac{dk'_x dk'_y dk'_z}{(2\pi)^3} f(q, k) \frac{q' - k'}{c_0 q' k' \sin \theta'} \delta(\theta'), \quad (\text{D21})$$

$$= \pi \frac{1}{c_x} \int \frac{k'^2 dk'}{4\pi^2} f(q, k) \frac{q' - k'}{q' k'}, \quad (\text{D22})$$

$$= \frac{c_\theta^2}{c_0^2 c_x} \int_0^q \frac{k^2 dk}{4\pi} \frac{k q^2 (q - k)}{2} \frac{q - k}{q k}, \quad (\text{D23})$$

$$= \frac{1}{2} \frac{c_\theta^2}{c_0^2 c_x} \frac{q^6}{120\pi}. \quad (\text{D24})$$

We now calculate $\Im \Sigma_{\phi\phi,2}(\varepsilon_{\text{ph}}(\mathbf{q}) + i0^+, \mathbf{q})$ at finite temperature,

$$\begin{aligned} \Im \Sigma_{\phi\phi,2}(\varepsilon_{\text{ph}}(\mathbf{q}) + i0^+, \mathbf{q}) &= \pi \sum_{\mathbf{k}} [n(\varepsilon_{\text{ph}}(\mathbf{k})) - n(\varepsilon_{\text{ph}}(\mathbf{q} - \mathbf{k}))] \left[(\mathbf{k} \cdot \mathbf{q})^2 \frac{B_{11}(\mathbf{k}) B_{22}(\mathbf{q} - \mathbf{k})}{4\varepsilon_{\text{ph}}(\mathbf{k}) \varepsilon_{\text{ph}}(\mathbf{q} - \mathbf{k})} \right. \\ &\quad \left. - \mathbf{k} \cdot \mathbf{q} (\mathbf{q}^2 - \mathbf{k} \cdot \mathbf{q}) \frac{B_{12}(\mathbf{k}) B_{12}(\mathbf{q} - \mathbf{k})}{4} \right] \\ &\quad \times [-\delta(\varepsilon_{\text{ph}}(\mathbf{q}) + \varepsilon_{\text{ph}}(\mathbf{q} - \mathbf{k}) - \varepsilon_{\text{ph}}(\mathbf{k})) + \delta(\varepsilon_{\text{ph}}(\mathbf{q}) + \varepsilon_{\text{ph}}(\mathbf{k}) - \varepsilon_{\text{ph}}(\mathbf{q} - \mathbf{k}))], \end{aligned} \quad (\text{D25})$$

$$= -\pi \sum_{\mathbf{k}} [n(\varepsilon_{\text{ph}}(\mathbf{k} + \mathbf{q})) - n(\varepsilon_{\text{ph}}(\mathbf{k}))] \delta(\varepsilon_{\text{ph}}(\mathbf{q}) + \varepsilon_{\text{ph}}(\mathbf{k}) - \varepsilon_{\text{ph}}(\mathbf{k} + \mathbf{q})) g(\mathbf{q}, \mathbf{k}), \quad (\text{D26})$$

$$= -\pi \sum_{\mathbf{k}} \frac{\partial n(\varepsilon_{\text{ph}}(\mathbf{k}))}{\partial \varepsilon_{\text{ph}}(\mathbf{k})} \varepsilon_{\text{ph}}(\mathbf{q}) \delta(\varepsilon_{\text{ph}}(\mathbf{q}) + \varepsilon_{\text{ph}}(\mathbf{k}) - \varepsilon_{\text{ph}}(\mathbf{k} + \mathbf{q})) g(\mathbf{q}, \mathbf{k}), \quad (\text{D27})$$

where

$$g(\mathbf{q}, \mathbf{k}) = \left[(\mathbf{k} \cdot \mathbf{q} + \mathbf{q}^2)^2 \frac{B_{11}(\mathbf{k} + \mathbf{q}) B_{22}(\mathbf{k})}{4\varepsilon_{\text{ph}}(\mathbf{k} + \mathbf{q}) \varepsilon_{\text{ph}}(\mathbf{k})} + (\mathbf{k} \cdot \mathbf{q} + \mathbf{q}^2) \mathbf{k} \cdot \mathbf{q} \frac{B_{12}(\mathbf{k} + \mathbf{q}) B_{12}(\mathbf{k})}{2} + (\mathbf{k} \cdot \mathbf{q})^2 \frac{B_{11}(\mathbf{k}) B_{22}(\mathbf{q} + \mathbf{k})}{4\varepsilon_{\text{ph}}(\mathbf{k}) \varepsilon_{\text{ph}}(\mathbf{q} + \mathbf{k})} \right]. \quad (\text{D28})$$

To get Eq. (D27) we have assumed $c_\theta q/T \ll 1$ and expand $n(\varepsilon_{\text{ph}}(\mathbf{k} + \mathbf{q})) - n(\varepsilon_{\text{ph}}(\mathbf{k}))$ to the lowest order. In general it is difficult to solve the energy and momentum conserving condition $\delta(\varepsilon_{\text{ph}}(\mathbf{q}) + \varepsilon_{\text{ph}}(\mathbf{k}) - \varepsilon_{\text{ph}}(\mathbf{k} + \mathbf{q}))$ even if \mathbf{q} is small, because \mathbf{k} is not necessarily small and for general \mathbf{k} , the phonon dispersion is very complicated. However, if we focus on the low-temperature region such that the corresponding phonon dispersion is linear, then we can replace $\varepsilon_{\text{ph}}(\mathbf{k})$ by the linear dispersion because $\frac{\partial n(\varepsilon_{\text{ph}}(\mathbf{k}))}{\partial \varepsilon_{\text{ph}}(\mathbf{k})}$ decays rapidly when $\varepsilon_{\text{ph}}(\mathbf{k}) > T$. In this region the momentum and energy conservation is easily solved: \mathbf{k} and \mathbf{q} are along the same direction and the length of \mathbf{k} is unrestricted. Under this condition $g(\mathbf{q}, \mathbf{k})$ also takes a simple form

$$g(\mathbf{q}, \mathbf{k}) = kq^2(k + q), \quad (\text{D29})$$

and

$$\Im \Sigma_{\phi\phi,2}[\varepsilon_{\text{ph}}(\mathbf{q}) + i0^+, \mathbf{q}] = \frac{c_\theta^2}{c_0^2 c_x} \int_0^\infty \frac{k^2 dk}{4\pi} \frac{\beta e^{\beta c_\theta k}}{(e^{\beta c_\theta k} - 1)^2} c_\theta q k q^2 (k + q) \frac{q + k}{q k}, \quad (\text{D30})$$

$$= \frac{q^2 T^4}{c_\theta^2 c_0^2 c_x} \int_0^\infty \frac{x^2 dx}{4\pi} \frac{e^x}{(e^x - 1)^2} \left(x + \frac{c_\theta q}{T}\right)^2, \quad (\text{D31})$$

$$= \frac{\pi^3 q^2 T^4}{15 c_\theta^2 c_0^2 c_x}. \quad (\text{D32})$$

To get Eq. (D32) from Eq. (D31), we have used the condition $c_\theta q/T \ll 1$.

We can calculate other self-energies in the similar way, and here we just summarize the final results,

$$\begin{aligned}
 \Im \Sigma_{\phi\phi,1} &= \frac{1}{2} \frac{c_\theta^2}{c_0^2 c_x} \frac{q^6}{120\pi} & \Im \Sigma_{\phi\phi,2} &= \frac{\pi^3 q^2 T^4}{15 c_\theta^2 c_0^2 c_x} \\
 \Re \Sigma_{\phi\zeta+,1} &= \frac{g_+}{4} \left[1 - \frac{2k_0^2 \Omega \cos^2 \theta}{(\Omega + 2G_2)^2} \right] \frac{c_\theta}{c_0^2 c_x} \frac{q^5}{120\pi} & \Re \Sigma_{\phi\zeta+,2} &= \frac{g_+}{2} \left[1 - \frac{2k_0^2 \Omega \cos^2 \theta}{(\Omega + 2G_2)^2} \right] \frac{1}{c_0^2 c_\theta^3 c_x} \frac{\pi^3 q T^4}{15} \\
 \Re \Sigma_{\zeta+\zeta+,1} &= \frac{g_+}{8\rho} \left[1 - \frac{2\Omega k_0^2 \cos^2 \theta}{(\Omega + 2G_2)^2} \right]^2 \frac{1}{c_x} \frac{q^4}{120\pi} & \Re \Sigma_{\zeta+\zeta+,2} &= \frac{g_+}{4\rho} \left[1 - \frac{2\Omega k_0^2 \cos^2 \theta}{(\Omega + 2G_2)^2} \right]^2 \frac{1}{c_\theta^4 c_x} \frac{\pi^3 T^4}{15} \\
 \Re \Sigma_{\zeta-\zeta-,1} &= \frac{k_0^2 \Omega^2 \cos^2 \theta}{2\rho^2 (\Omega + 2G_2)^2} \frac{c_\theta^2}{c_0^2 c_x} \frac{q^4}{120\pi} & \Re \Sigma_{\zeta-\zeta-,2} &= \frac{k_0^2 \Omega^2 \cos^2 \theta}{\rho^2 (\Omega + 2G_2)^2} \frac{1}{c_0^2 c_\theta^2 c_x} \frac{\pi^3 T^4}{15} \\
 \Re \Sigma_{\phi\zeta-,1} &= \frac{\Omega k_0 \cos \theta}{2\rho (\Omega + 2G_2)} \frac{c_\theta^2}{c_0^2 c_x} \frac{q^5}{120\pi} & \Re \Sigma_{\phi\zeta-,2} &= \frac{\Omega k_0 \cos \theta}{\rho (\Omega + 2G_2)} \frac{1}{c_0^2 c_\theta^2 c_x} \frac{\pi^3 q T^4}{15} \\
 \Re \Sigma_{\zeta+\zeta-,1} &= \frac{g_+ \Omega k_0 \cos \theta}{4\rho (\Omega + 2G_2)} \left[1 - \frac{2k_0^2 \Omega \cos^2 \theta}{(\Omega + 2G_2)^2} \right] \frac{c_\theta}{c_0^2 c_x} \frac{q^4}{120\pi} & \Re \Sigma_{\zeta+\zeta-,2} &= \frac{g_+ \Omega k_0 \cos \theta}{2\rho (\Omega + 2G_2)} \left[1 - \frac{2k_0^2 \Omega \cos^2 \theta}{(\Omega + 2G_2)^2} \right] \frac{1}{c_0^2 c_\theta^3 c_x} \frac{\pi^3 T^4}{15}
 \end{aligned} \tag{D33}$$

From the above results we get the Beliaev damping rate at zero temperature

$$\gamma_B = \frac{3g_+ q^5}{640\pi c_\theta} \left[1 - \frac{2\Omega k_0^2 \cos^2 \theta}{(\Omega + 2G_2)^2} \right]^2 \frac{c_\theta^2}{c_0^2 c_x}, \tag{D34}$$

$$= \frac{3q^5}{640\pi \rho} \left[1 - \frac{2\Omega k_0^2 \cos^2 \theta}{(\Omega + 2G_2)^2} \right]^2 \frac{c_\theta}{c_x}, \tag{D35}$$

$$= \frac{3q^5}{640\pi \rho} \left[1 - \frac{2\Omega k_0^2 \cos^2 \theta}{(\Omega + 2G_2)^2} \right]^2 \sqrt{1 + \frac{2k_0^2 \sin^2 \theta}{\Omega + 2G_2 - 2k_0^2}} \tag{D36}$$

and the Landau damping rate at finite temperature

$$\gamma_L = \frac{3\pi^3 q T^4}{40\rho c_\theta^4} \left[1 - \frac{2\Omega k_0^2 \cos^2 \theta}{(\Omega + 2G_2)^2} \right]^2 \sqrt{1 + \frac{2k_0^2 \sin^2 \theta}{\Omega + 2G_2 - 2k_0^2}}. \tag{D37}$$

The Beliaev damping rate takes the same form as the result in Ref. [41], where a different method was used. The analytical expression for the Landau damping rate is obtained here for the first time.

If $G_2 = g_- \rho = 0$, the damping rates can be further simplified as

$$\gamma_B = \frac{3q^5}{640\pi \rho} \frac{c_\theta^4}{c_0^4} \sqrt{1 + \frac{2k_0^2 \sin^2 \theta}{\Omega - 2k_0^2}}, \tag{D38}$$

$$\gamma_L = \frac{3\pi^3 q T^4}{40\rho c_0^4} \sqrt{1 + \frac{2k_0^2 \sin^2 \theta}{\Omega - 2k_0^2}}. \tag{D39}$$

Since $c_\theta = c_0 \sqrt{1 - \frac{2k_0^2 \cos^2 \theta}{\Omega + 2G_2}}$, the Beliaev damping is strongly suppressed when the momentum is along the direction of the spin-orbit coupling. However, the Landau damping is not suppressed.

-
- [1] M. Z. Hasan and C. L. Kane, Colloquium: Topological insulators, *Rev. Mod. Phys.* **82**, 3045 (2010).
- [2] X.-L. Qi and S.-C. Zhang, Topological insulators and superconductors, *Rev. Mod. Phys.* **83**, 1057 (2011).
- [3] B. Yan and C. Felser, Topological materials: Weyl semimetals, *Annu. Rev. Condens. Matter Phys.* **8**, 337 (2017).
- [4] N. P. Armitage, E. J. Mele, and A. Vishwanath, Weyl and Dirac semimetals in three-dimensional solids, *Rev. Mod. Phys.* **90**, 015001 (2018).
- [5] S. R. Elliott and M. Franz, Colloquium: Majorana fermions in nuclear, particle, and solid-state physics, *Rev. Mod. Phys.* **87**, 137 (2015).
- [6] Ch. Rüegg, N. Cavadin, A. Furrer, H.-U. Güdel, K. Krämer, H. Mutka, A. Wildes, K. Habicht, and P. Vorderwisch, Bose-Einstein condensation of the triplet states in the magnetic insulator TiCuCl_3 , *Nature (London)* **423**, 62 (2003).
- [7] J. Sirker, A. Weiße, and O. P. Sushkov, Consequences of spin-orbit coupling for the Bose-Einstein condensation of magnons, *Europhys. Lett.* **68**, 275 (2004).
- [8] S. O. Demokritov, V. E. Demidov, O. Dzyapko, G. A. Melkov, A. A. Serga, B. Hillebrands, and A. N. Slavin, Bose-Einstein condensation of quasi-equilibrium magnons at room temperature under pumping, *Nature (London)* **443**, 430 (2006).
- [9] T. Hakioglu and M. Şahin, Excitonic Condensation under Spin-Orbit Coupling and BEC-BCS Crossover, *Phys. Rev. Lett.* **98**, 166405 (2007).

- [10] M. A. Can and T. Hakioglu, Unconventional Pairing in Excitonic Condensates under Spin-Orbit Coupling, *Phys. Rev. Lett.* **103**, 086404 (2009).
- [11] A. A. High, J. R. Leonard, A. T. Hammack, M. M. Fogler, L. V. Butov, A. V. Kavokin, K. L. Campman, and A. C. Gossard, Spontaneous coherence in a cold exciton gas, *Nature (London)* **483**, 584 (2012).
- [12] A. A. High, A. T. Hammack, J. R. Leonard, S. Yang, L. V. Butov, T. Ostatnický, M. Vladimirova, A. V. Kavokin, T. C. H. Liew, K. L. Campman, and A. C. Gossard, Spin Currents in a Coherent Exciton Gas, *Phys. Rev. Lett.* **110**, 246403 (2013).
- [13] I. Carusotto and C. Ciuti, Quantum fluids of light, *Rev. Mod. Phys.* **85**, 299 (2013).
- [14] T. Byrnes, N. Y. Kim, and Y. Yamamoto, Exciton-polariton condensates, *Nat. Phys.* **10**, 803 (2014).
- [15] V. G. Sala, D. D. Solnyshkov, I. Carusotto, T. Jacqmin, A. Lemaître, H. Terças, A. Nalitov, M. Abbarchi, E. Galopin, I. Sagnes, J. Bloch, G. Malpuech, and A. Amo, Spin-Orbit Coupling for Photons and Polaritons in Microstructures, *Phys. Rev. X* **5**, 011034 (2015).
- [16] C. E. Whittaker, E. Cancellieri, P. M. Walker, D. R. Gulevich, H. Schomerus, D. Vaitiekus, B. Royall, D. M. Whittaker, E. Clarke, I. V. Iorsh, I. A. Shelykh, M. S. Skolnick, and D. N. Krizhanovskii, Exciton Polaritons in a Two-Dimensional Lieb Lattice with Spin-Orbit Coupling, *Phys. Rev. Lett.* **120**, 097401 (2018).
- [17] S. Klembt, T. H. Harder, O. A. Egorov, K. Winkler, H. Suchomel, J. Beierlein, M. Emmerling, C. Schneider, and S. Höfling, Polariton condensation in S- and P-flatbands in a two-dimensional Lieb lattice, *Appl. Phys. Lett.* **111**, 231102 (2017).
- [18] D. A. Zezyulin, Y. V. Kartashov, D. V. Skryabin, and I. A. Shelykh, Spin-orbit coupled polariton condensates in a radially periodic potential: Multiring vortices and rotating solitons, *ACS Photonics* **5**, 3634 (2018).
- [19] Y. J. Lin, K. Jiménez-García, and I. B. Spielman, Spin-orbit-coupled Bose-Einstein condensates, *Nature (London)* **471**, 83 (2011).
- [20] J.-Y. Zhang, S.-C. Ji, Z. Chen, L. Zhang, Z.-D. Du, B. Yan, G.-S. Pan, B. Zhao, Y.-J. Deng, H. Zhai, S. Chen, and J.-W. Pan, Collective Dipole Oscillations of a Spin-Orbit Coupled Bose-Einstein Condensate, *Phys. Rev. Lett.* **109**, 115301 (2012).
- [21] S.-C. Ji, L. Zhang, X.-T. Xu, Z. Wu, Y. Deng, S. Chen, and J.-W. Pan, Softening of Roton and Phonon Modes in a Bose-Einstein Condensate with Spin-Orbit Coupling, *Phys. Rev. Lett.* **114**, 105301 (2015).
- [22] Z. Wu, L. Zhang, W. Sun, X.-T. Xu, B.-Z. Wang, S.-C. Ji, Y. Deng, S. Chen, X.-J. Liu, and J.-W. Pan, Realization of two-dimensional spin-orbit coupling for Bose-Einstein condensates, *Science* **354**, 83 (2016).
- [23] F. Dalfovo, S. Giorgini, L. P. Pitaevskii, and S. Stringari, Theory of Bose-Einstein condensation in trapped gases, *Rev. Mod. Phys.* **71**, 463 (1999).
- [24] J. Kasprzak, M. Richard, S. Kundermann, A. Baas, P. Jembrun, J. M. J. Keeling, F. M. Marchetti, M. H. Szymanska, R. André, J. L. Staehli, V. Savona, P. B. Littlewood, B. Deveaud, and L. S. Dang, Bose-Einstein condensation of exciton polaritons, *Nature (London)* **443**, 409 (2006).
- [25] R. Balili, V. Hartwell, D. Snoko, L. Pfeiffer, and K. West, Bose-Einstein condensation of microcavity polaritons in a trap, *Science* **316**, 1007 (2007).
- [26] S. R. K. Rodriguez, W. Casteels, F. Storme, N. Carlon Zambon, I. Sagnes, L. Le Gratiet, E. Galopin, A. Lemaître, A. Amo, C. Ciuti, and J. Bloch, Probing a Dissipative Phase Transition via Dynamical Optical Hysteresis, *Phys. Rev. Lett.* **118**, 247402 (2017).
- [27] T. Fink, A. Schade, S. Höfling, C. Schneider, and A. Imamoglu, Signatures of a dissipative phase transition in photon correlation measurements, *Nat. Phys.* **14**, 365 (2018).
- [28] S. B. Papp, J. M. Pino, R. J. Wild, S. Ronen, C. E. Wieman, D. S. Jin, and E. A. Cornell, Bragg Spectroscopy of a Strongly Interacting ^{85}Rb Bose-Einstein Condensate, *Phys. Rev. Lett.* **101**, 135301 (2008).
- [29] S. E. Pollack, D. Dries, M. Junker, Y. P. Chen, T. A. Corcovilos, and R. G. Hulet, Extreme Tunability of Interactions in a ^7Li Bose-Einstein Condensate, *Phys. Rev. Lett.* **102**, 090402 (2009).
- [30] N. Navon, S. Piatecki, K. Günter, B. Rem, T. C. Nguyen, F. Chevy, W. Krauth, and C. Salomon, Dynamics and Thermodynamics of the Low-Temperature Strongly Interacting Bose Gas, *Phys. Rev. Lett.* **107**, 135301 (2011).
- [31] D. S. Petrov, Quantum Mechanical Stabilization of a Collapsing Bose-Bose Mixture, *Phys. Rev. Lett.* **115**, 155302 (2015).
- [32] Y. Li, Z. Luo, Y. Liu, Z. Chen, C. Huang, S. Fu, H. Tan, and B. A. Malomed, Two-dimensional solitons and quantum droplets supported by competing self- and cross-interactions in spin-orbit-coupled condensates, *New J. Phys.* **19**, 113043 (2017).
- [33] C. R. Cabrera, L. Tanzi, J. Sanz, B. Naylor, P. Thomas, P. Cheiney, and L. Tarruell, Quantum liquid droplets in a mixture of Bose-Einstein condensates, *Science* **359**, 301 (2018).
- [34] G. Semeghini, G. Ferioli, L. Masi, C. Mazzinghi, L. Wolswijk, F. Minardi, M. Modugno, G. Modugno, M. Inguscio, and M. Fattori, Self-Bound Quantum Droplets of Atomic Mixtures in Free Space, *Phys. Rev. Lett.* **120**, 235301 (2018).
- [35] N. B. Jørgensen, G. M. Bruun, and J. J. Arlt, Dilute Fluid Governed by Quantum Fluctuations, *Phys. Rev. Lett.* **121**, 173403 (2018).
- [36] H. Zhai, Degenerate quantum gases with spin-orbit coupling: A review, *Rep. Prog. Phys.* **78**, 026001 (2015).
- [37] T. Ozawa and G. Baym, Stability of Ultracold Atomic Bose Condensates with Rashba Spin-Orbit Coupling Against Quantum and Thermal Fluctuations, *Phys. Rev. Lett.* **109**, 025301 (2012).
- [38] X. Cui and Q. Zhou, Enhancement of condensate depletion due to spin-orbit coupling, *Phys. Rev. A* **87**, 031604(R) (2013).
- [39] W. Zheng, Z.-Q. Yu, X. Cui, and H. Zhai, Properties of Bose gases with the Raman-induced spin-orbit coupling, *J. Phys. B* **46**, 134007 (2013).
- [40] E. Kawasaki and M. Holzmann, Finite-temperature phases of two-dimensional spin-orbit-coupled bosons, *Phys. Rev. A* **95**, 051601(R) (2017).
- [41] R. Wu and Z. Liang, Beliaev Damping of a Spin-Orbit-Coupled Bose-Einstein Condensate, *Phys. Rev. Lett.* **121**, 180401 (2018).

- [42] Y. Li, L. P. Pitaevskii, and S. Stringari, Quantum Tricriticality and Phase Transitions in Spin-Orbit Coupled Bose-Einstein Condensates, *Phys. Rev. Lett.* **108**, 225301 (2012).
- [43] P. Wang, Z.-Q. Yu, Z. Fu, J. Miao, L. Huang, S. Chai, H. Zhai, and J. Zhang, Spin-Orbit Coupled Degenerate Fermi Gases, *Phys. Rev. Lett.* **109**, 095301 (2012).
- [44] L. W. Cheuk, A. T. Sommer, Z. Hadzibabic, T. Yefsah, W. S. Bakr, and M. W. Zwierlein, Spin-Injection Spectroscopy of a Spin-Orbit Coupled Fermi Gas, *Phys. Rev. Lett.* **109**, 095302 (2012).
- [45] C. H. L. Quay, T. L. Hughes, J. A. Sulpizio, L. N. Pfeiffer, K. W. Baldwin, K. W. West, D. Goldhaber-Gordon, and R. de Picciotto, Observation of a one-dimensional spin-orbit gap in a quantum wire, *Nat. Phys.* **6**, 336 (2010).
- [46] V. Mourik, K. Zuo, S. M. Frolov, S. R. Plissard, E. P. A. M. Bakkers, and L. P. Kouwenhoven, Signatures of Majorana fermions in hybrid superconductor-semiconductor nanowire devices, *Science* **336**, 1003 (2012).
- [47] A. Das, Y. Ronen, Y. Most, Y. Oreg, M. Heiblum, and H. Shtrikman, Zero-bias peaks and splitting in an Al-InAs nanowire topological superconductor as a signature of Majorana fermions, *Nature Phys.* **8**, 887 (2012).
- [48] G. I. Martone, Y. Li, L. P. Pitaevskii, and S. Stringari, Anisotropic dynamics of a spin-orbit-coupled Bose-Einstein condensate, *Phys. Rev. A* **86**, 063621 (2012).
- [49] Y. Li, G. I. Martone, and S. Stringari, Sum rules, dipole oscillation and spin polarizability of a spin-orbit coupled quantum gas, *Europhys. Lett.* **99**, 56008 (2012).
- [50] Y.-C. Zhang, Z.-Q. Yu, T. K. Ng, S. Zhang, L. Pitaevskii, and S. Stringari, Superfluid density of a spin-orbit-coupled Bose gas, *Phys. Rev. A* **94**, 033635 (2016).
- [51] T. D. Lee, K. Huang, and C. N. Yang, Eigenvalues and eigenfunctions of a Bose system of hard spheres and its low-temperature properties, *Phys. Rev.* **106**, 1135 (1957).
- [52] J. O. Andersen, Theory of the weakly interacting Bose gas, *Rev. Mod. Phys.* **76**, 599 (2004).
- [53] A. J. Leggett, On the Superfluid Fraction of an Arbitrary Many-Body System at $T=0$, *J. Stat. Phys.* **93**, 927 (1998).
- [54] X.-L. Chen, X.-J. Liu, and H. Hu, Quantum and thermal fluctuations in a Raman spin-orbit-coupled Bose gas, *Phys. Rev. A* **96**, 013625 (2017).
- [55] S. T. Beliaev, Energy-spectrum of a non-ideal Bose gas, *J. Exptl. Theor. Phys. (U.S.S.R.)* **34**, 433 (1958) [*Sov. Phys. JETP* **7**, 299 (1958)].
- [56] P. C. Hohenberg and P. C. Martin, Microscopic theory of superfluid helium, *Ann. Phys. (NY)* **34**, 291 (1965).
- [57] L. P. Pitaevskii and S. Stringari, Landau damping in dilute Bose gases, *Phys. Lett. A* **235**, 398 (1997).
- [58] W. V. Liu, Theoretical Study of the Damping of Collective Excitations in a Bose-Einstein Condensate, *Phys. Rev. Lett.* **79**, 4056 (1997).
- [59] P. O. Fedichev, G. V. Shlyapnikov, and J. T. M. Walraven, Damping of Low-Energy Excitations of a Trapped Bose-Einstein Condensate at Finite Temperatures, *Phys. Rev. Lett.* **80**, 2269 (1998).